REPORT NO.
UCB/SEMM-89/24

STRUCTURAL ENGINEERING,
MECHANICS AND MATERIALS

A MODIFIED CAP MODEL: CLOSEST POINT SOLUTION ALGORITHMS

by

G. HOFSTETTER
J.C. SIMO
R.L. TAYLOR

DECEMBER 1989

DEPARTMENT OF CIVIL ENGINEERING
UNIVERSITY OF CALIFORNIA AT BERKELEY
BERKELEY, CALIFORNIA

A MODIFIED CAP MODEL: CLOSEST POINT SOLUTION ALGORITHMS

G. Hofstetter[1], J.C. Simo[2] and R.L. Taylor[3]

ABSTRACT

An application of the return mapping algorithm for the inviscid two invariant cap model, originally proposed by DiMaggio and Sandler, is presented. This cap model serves as an example for nonsmooth multisurface plasticity. Precise conditions for discrete loading in all possible modes are derived from the discrete Kuhn-Tucker conditions and new unconditionally stable closest point projection algorithms are presented. These are characterized by reducing local iterations on the constitutive equations to the solution of one nonlinear scalar equation for each of the different modes of the cap model. Tangent operators, consistent with the integration algorithm are derived, thus preserving the quadratic rate of convergence in a Newton solution procedure. It is shown that the original cap model does not obey the principle of maximum plastic dissipation, because the hardening law for the cap is nonassociative, which leads to the undesirable feature of unsymmetric consistent tangent moduli. To overcome this drawback an associative hardening law is proposed for a restricted class of problems.

1. INTRODUCTION

The cap model, originally proposed by DiMaggio and Sandler [1] (see also Sandler, DiMaggio and Baladi [2]), allows the control of dilatancy by means of a hardening cap that intersects a fixed failure envelope in a nonsmooth fashion. A commonly accepted interpretation of this model (see, e.g. Chen [3], Chen and Baladi [4], Desai and Siriwardane [5] or Simo, Ju, Pister and Taylor [6]) assumes a one-to-one correspondence between hardening of the cap and plastic volume change. However, if a one-to-one hardening law is postulated, softening response may occur when the stress point is located at the compressive corner region. Motivated by this softening behavior, Sandler and Rubin [7] proposed a modified hardening law which prevents softening response.

The main thrust of our work is the development of a systematic algorithmic treatment of the cap model within the framework of the closest point projection algorithms. In particular we consider the following aspects:

i) The functional form for the cap is reformulated to make it suitable for the application of a closest point projection algorithm.

ii) Consistent algorithmic loading/unloading conditions for all possible modes of response are precisely formulated by exploiting appropiate discrete Kuhn-Tucker conditions. As recently shown in Simo et al. [8] the Kuhn-Tucker conditions lead to a useful characterization of plastic loading for multisurface plasticity in an algorithmic context.

iii) Return mapping algorithms are formulated for the tension cutoff, tension cutoff corner, failure, cap and compressive corner modes by a straightforward application of an implicit backward Euler integration scheme based on Koiter's generalized flow rule [9]. In particular, new closest point projection schemes, characterized by reducing local iterations to the solution of one nonlinear scalar equation, are presented for loading in the cap and failure modes. These exhibit quadratic rate of convergence, whereas the secant iteration scheme proposed by Sandler and Rubin [7] is only superlinear.

iv) Based on the general return mapping algorithm for nonsmooth multisurface plasticity (see Simo et al. [8]) consistent tangent moduli for the cap model are derived. When used with a Newton type solution these preserve a quadratic rate of convergence. All the steps

1. Visiting Scholar, Department of Civil Engineering, University of California at Berkeley.
2. Associate Professor, Division of Applied Mechanics, Stanford University
3. Professor, Department of Civil Engineering, University of California at Berkeley.

to obtain the so called algorithmic moduli are performed algebraically, thus avoiding time consuming numerical inversions.

v) It will be shown, that the commonly accepted hardening law [3, 4, 5, 6] for the cap model is nonassociative in the sense that it is not derived from a potential [10]. To overcome the drawback of nonsymmetric consistent tangent moduli, caused by the nonassociative hardening law, an associative hardening law is proposed.

vi) The effectiveness of the proposed algorithms is demonstrated numerically.

2. FORMULATION OF THE CAP MODEL

The two invariant, rate independent cap model is defined by a convex yield surface, which consists of a failure envelope $f_1(\sigma)$, an elliptical cap $f_2(\sigma,\kappa)$ and a tension cutoff region $f_3(\sigma)$, where σ denotes the stress tensor and κ is the hardening parameter. In contrast to the strain hardening cap, the failure envelope and the tension cutoff region are characterized as ideal plasticity surfaces. The functional forms for these surfaces are (Fig. 1):

$$f_1(\sigma) = |s| - F_e(I_1) \quad \text{for } T \le I_1 < \kappa \tag{1}$$

where

$$F_e(I_1) = \alpha - \lambda \exp^{-\beta I_1} + \theta I_1, \tag{2}$$

$$f_2(\sigma,\kappa) = F_c(|s|, I_1, \kappa) - F_e(\kappa) \quad \text{for } \kappa \le I_1 \le X(\kappa) \tag{3}$$

where

$$F_c(|s|, I_1, \kappa) = \left[|s|^2 + \frac{1}{R^2}(I_1 - L(\kappa))^2 \right]^{1/2} \tag{4}$$

$$f_3(\sigma) = T - I_1 \quad \text{for } I_1 = T \tag{5}$$

where α, β, λ, θ and R are material parameters for the cap and failure envelope; T is a material constant referred to as the tension cutoff; I_1 and $|s|$ are the first invariant of the stress tensor σ and the norm of the deviatoric stress tensor s, respectively. The deviator stress, s, is defined as

$$s = \sigma - \frac{1}{3} I_1 \mathbf{1} \tag{6}$$

where $\mathbf{1}$ is the second order unit tensor. Thus, $I_1 = tr(\sigma)$ and the norm of s is $|s| = \sqrt{s:s}$. In (4) $L(\kappa)$ is defined as

$$L(\kappa) = <\kappa> = \begin{cases} \kappa & \text{if } \kappa > 0 \\ 0 & \text{if } \kappa \le 0 \end{cases} \tag{7}$$

Following standard conventions in soil mechanics, compression and compaction is assumed to be positive. The point of intersection of the cap with the I_1 - axis is defined as

$$X(\kappa) = \kappa + R F_e(\kappa) \tag{8}$$

The functional form for the cap (3) differs from the form given in Sandler and Rubin [7] or Simo, Ju, Pister and Taylor [6], where

$$f_2(\sigma,\kappa) = \sqrt{J_{2D}} - \frac{1}{R}\sqrt{[X(\kappa) - L(\kappa)]^2 - [I_1 - L(\kappa)]^2} \tag{9}$$

For comparison of (9) and (3) we note that

$$F_e(\kappa) = \frac{X(\kappa) - L(\kappa)}{R}, \quad |\mathbf{s}| = \sqrt{2J_{2D}}$$

Application of the closest point projection algorithm may lead to trial values for I_1, which are greater than X(κ). In this case (9) leads to a square root of a negative number and may not be used in the context with a closest point algorithm. Use of (3) leads to a failure surface with similar functional form to (9) but avoiding possibility of the negative square root.

Analogous to (6) the deviatoric strain tensor **e** is defined as

$$\mathbf{e} = \boldsymbol{\epsilon} - \frac{1}{3}\bar{I}_1\mathbf{1} \tag{10}$$

where $\boldsymbol{\epsilon}$ denotes the strain tensor and $\bar{I}_1 = \mathrm{tr}(\boldsymbol{\epsilon})$. The hardening parameter is implicitely defined as a functional of the plastic volumetric strain $\bar{I}_1^P$. Sandler and Rubin [7] propose a relationship whose qualitative shape is deduced from a hydrostatic test

$$\bar{\epsilon}_V^P = W\left(1 - \exp^{-D\,X(\kappa)}\right) \tag{11}$$

in which W and D are material parameters and $\bar{\epsilon}_V^P$ is the effective volumetric plastic strain, defined by integrating

$$\dot{\bar{\epsilon}}_V^P = \begin{cases} \dot{\bar{I}}_1^P & \text{if } \dot{\bar{I}}_1^P > 0 \text{ or } \kappa > 0 \text{ and } \kappa > I_1 \\ 0 & \text{otherwise} \end{cases} \tag{12}$$

According to this proposal, if the stress point is at the compressive corner point, movement of the cap is prevented and the model behaves as in perfect plasticity, thus avoiding a softening response.

The form of the elastic domain is defined in terms of the three yield surfaces as

$$f_1(\sigma) < 0 \text{ and } f_2(\sigma,\kappa) < 0 \text{ and } f_3(\sigma) < 0 \tag{13}$$

For multisurface plasticity an appropiate statement of the flow rule relies on Koiter's generalization [9] which in the present case of an associative flow rule takes the form

$$\dot{\boldsymbol{\epsilon}}^P = \sum_{i=1}^{3} \dot{\gamma}_i \frac{\partial f_i}{\partial \sigma} \tag{14}$$

where $\dot{\gamma}_i$, i = 1,2,3, are the plastic consistency parameters. Plastic loading or elastic loading/unloading is formulated in Kuhn-Tucker form by means of the relations (see Simo et al. [8])

$$\dot{\gamma}_i \geq 0, \quad f_i \leq 0 \text{ and } \dot{\gamma}_i f_i = 0, \quad i = 1,2,3. \tag{15}$$

This form of the loading/unloading conditions is standard and plays a fundamental role in subsequent

developments.

3. INTEGRATION ALGORITHM

3.1. Return Mapping Algorithm

The return mapping algorithm [11, 12] basically consists of two major steps, the formulation of the elastic trial stress σ_{n+1}^{Trial}, also referred to as an elastic predictor and the return mapping to the yield surface, which can be interpreted as a closest point projection of the trial stress onto the yield surface, also referred to as a plastic corrector. For multisurface plasticity application of an implicit backward Euler integration scheme on the generalized flow rule (14) yields the following return mapping algorithm

$$\epsilon_{n+1}^{P} = \epsilon_{n}^{P} + \Delta\epsilon_{n+1}^{P} = \epsilon_{n}^{P} + \sum_{i=1}^{3} \Delta\gamma_{i,n+1} \frac{\partial f_{i,n+1}}{\partial \sigma_{n+1}}$$

$$\sigma_{n+1}^{Trial} = \mathbf{C} : (\epsilon_{n+1} - \epsilon_{n}^{P}) \tag{16}$$

$$\sigma_{n+1} = \mathbf{C} : (\epsilon_{n+1} - \epsilon_{n+1}^{P}) = \sigma_{n+1}^{Trial} - \mathbf{C} : \Delta\epsilon_{n+1}^{P}$$

where $\Delta\gamma_{i,n+1} = \Delta t\, \dot{\gamma}_{i,n+1}$ and $\mathbf{C}$ is the elasticity tensor. In addition, from (15) one obtains the discrete Kuhn-Tucker conditions that govern the evolution of the discrete consistency parameters $\Delta\gamma_{i,n+1}$

$$\Delta\gamma_{i,n+1} \geq 0,\ f_{i,n+1} \leq 0 \text{ and } \Delta\gamma_{i,n+1} f_{i,n+1} = 0, \qquad i = 1,2,3. \tag{17}$$

As in single surface plasticity plastic loading can be characterized in an algorithmic context solely on the basis of the elastic trial stress due to the convexity assumption on f_i. To this end one computes

$$f_{1,n+1}^{Trial} = f_{1,n+1}^{Trial}\ (|\mathbf{s}_{n+1}^{Trial}|, I_{1,n+1}^{Trial})$$

$$f_{2,n+1}^{Trial} = f_{2,n+1}^{Trial}\ (|\mathbf{s}_{n+1}^{Trial}|, I_{1,n+1}^{Trial}, \kappa_n) \tag{18}$$

$$f_{3,n+1}^{Trial} = f_{3,n+1}^{Trial}\ (I_{1,n+1}^{Trial})$$

where

$$\mathbf{s}_{n+1}^{Trial} = 2G(\mathbf{e}_{n+1} - \mathbf{e}_{n}^{P}) \qquad I_{1,n+1}^{Trial} = 3K(\bar{I}_{1,n+1} - \bar{I}_{1,n}^{P}) \tag{19}$$

It is intuitively clear and can be shown (Simo and Hughes [10]) that the convexity assumption implies $f_{i,n+1} \leq f_{i,n+1}^{Trial}$, i = 1,2,3. Thus from conditions (18) it follows that

$$f_{i,n+1}^{Trial} < 0 \rightarrow f_{i,n+1} < 0 \rightarrow \Delta\gamma_{i,n+1} = 0, \qquad i = 1,2,3, \tag{20}$$

and, thus, the process is elastic. On the other hand, if $f_{i,n+1}^{Trial} > 0$ for some i $\in$ [1,2,3] then the

process is plastic. In this latter case it is necessary to determine $\Delta\epsilon^P_{n+1}$ (or $\Delta\mathbf{e}^P_{n+1}$ and $\Delta\bar{I}^P_{1,n+1}$) and κ_{n+1}. Finally, the stresses are obtained from (16_3)

$$\mathbf{s}_{n+1} = \mathbf{s}^{Trial}_{n+1} - 2G\,\Delta\mathbf{e}^P_{n+1} \qquad I_{1,n+1} = I^{Trial}_{1,n+1} - 3K\,\Delta\bar{I}^P_{1,n+1} \tag{21}$$

3.2. Loading in the Various Modes of the Cap Model

In the following sections the return mapping algorithm for the different modes of the cap model, (consisting of the failure envelope mode, cap mode, tension cutoff mode, the compressive corner mode at $I_1 = \kappa$, and the tensile corner mode at $I_1 = T$) is described in detail. The conditions that characterize loading in each mode are deduced from the discrete Kuhn-Tucker conditions.

3.2.1. Loading in the failure envelope mode

Loading in the failure envelope mode is characterized by $f^{Trial}_{1,n+1} > 0$, $\Delta\gamma_{1,n+1} > 0$ and $\Delta\gamma_{2,n+1} = \Delta\gamma_{3,n+1} = 0$. From eqs.($16_1$), (1) and (2) one obtains

$$\Delta\mathbf{e}^P_{n+1} = \Delta\gamma_{1,n+1}\mathbf{n}_{n+1}, \qquad \mathbf{n}_{n+1} = \frac{\mathbf{s}_{n+1}}{|\mathbf{s}_{n+1}|}$$

$$\Delta\bar{I}^P_{1,n+1} = -3\Delta\gamma_{1,n+1}\frac{dF_e(I_1)}{dI_1} \tag{22}$$

Substituting eqs.(22) into (21), noting that (see Simo and Taylor [11])

$$\mathbf{n}_{n+1} = \frac{\mathbf{s}_{n+1}}{|\mathbf{s}_{n+1}|} = \frac{\mathbf{s}^{Trial}_{n+1}}{|\mathbf{s}^{Trial}_{n+1}|} \tag{23}$$

and adding the desired condition $f_{1,n+1} = 0$ (1), we can write

$$\begin{aligned} |\mathbf{s}_{n+1}| &= |\mathbf{s}^{Trial}_{n+1}| - 2G\,\Delta\gamma_{1,n+1} \\ I_{1,n+1} &= I^{Trial}_{1,n+1} + 9K\,\Delta\gamma_{1,n+1}\frac{dF_e}{dI_1} \\ |\mathbf{s}_{n+1}| &= F_e(I_{1,n+1}) \end{aligned} \tag{24}$$

These three equations can be combined into a nonlinear scalar equation for $I_{1,n+1}$

$$I^{Trial}_{1,n+1} + 9K\,\Delta\gamma_{1,n+1}\frac{dF_e}{dI_1} - I_{1,n+1} = 0 \tag{25}$$

where

$$\Delta\gamma_{1,n+1} = \frac{|\mathbf{s}^{Trial}_{n+1}| - F_e(I_{1,n+1})}{2G}\,, \tag{26}$$

which can be solved by a Newton iteration technique. Once $I_{1,n+1}$ is known, $\Delta\gamma_{1,n+1}$ and the stress

can be calculated. Note, that the hardening law is not involved in this stress update. The update procedure for the hardening parameter κ will be discussed in section 3.2.6.

3.2.2. Loading in the tension cutoff mode

Loading in the tension cutoff mode is characterized by $f^{Trial}_{3,n+1} > 0$, $\Delta\gamma_{3,n+1} > 0$ and $\Delta\gamma_{1,n+1} = \Delta\gamma_{2,n+1} = 0$. From (16_1) and (5) we obtain

$$\Delta\mathbf{e}^{P}_{n+1} = 0, \quad \Delta\bar{I}^{P}_{1,n+1} = -3\Delta\gamma_{3,n+1} \tag{27}$$

Since $I_{1,n+1} = T$, substitution of (27) into (21) yields $\mathbf{s}_{n+1} = \mathbf{s}^{Trial}_{n+1}$ and

$$\Delta\gamma_{3,n+1} = \frac{T - I^{Trial}_{1,n+1}}{9K} \tag{28}$$

Again, the update of the hardening parameter is not involved in the determination of the stress.

3.2.3. Loading in the tensile corner region

Loading in this corner region requires that $\Delta\gamma_{1,n+1} > 0$, $\Delta\gamma_{3,n+1} > 0$ and $\Delta\gamma_{2,n+1} = 0$. Note that in multisurface plasticity, if more than one yield criterion is active, then $f^{Trial}_{i,n+1} > 0$ does not necessarily imply that $\Delta\gamma_{i,n+1} > 0$ (see Simo et al. [8]). Consequently the discrete version of Koiter's generalized flow rule (16_1) yields

$$\begin{aligned} \Delta\mathbf{e}^{P}_{n+1} &= \Delta\gamma_{1,n+1}\mathbf{n}_{n+1} \\ \Delta\bar{I}^{P}_{1,n+1} &= -3\left(\Delta\gamma_{1,n+1}\frac{dF_e(T)}{dI_1} + \Delta\gamma_{3,n+1}\right) \end{aligned} \tag{29}$$

Since both the failure envelope and the tension cutoff surface behave as in ideal plasticity, the return point $\boldsymbol{\sigma}_{n+1}$ is the intersection of these two surfaces

$$I_{1,n+1} = T, \quad |\mathbf{s}_{n+1}| = F_e(T) \tag{30}$$

Substituting eqs.(30) and (29) into (21) and consideration of (23) give

$$\begin{aligned} \Delta\gamma_{1,n+1} &= \frac{|\mathbf{s}^{Trial}_{n+1}| - F_e(T)}{2G} \\ \Delta\gamma_{3,n+1} &= \frac{T - I^{Trial}_{1,n+1}}{9K} - \Delta\gamma_{1,n+1}\frac{dF_e(T)}{dI_1} \end{aligned} \tag{31}$$

Since $f^{Trial}_{3,n+1} > 0$ and enforcing $\Delta\gamma_{1,n+1} > 0$ and $\Delta\gamma_{3,n+1} > 0$ we obtain the inequalities that characterize loading within the corner region at $I_1 = T$

$$I^{Trial}_{1,n+1} < T \quad \text{and} \quad F_e(T) < |\mathbf{s}^{Trial}_{n+1}| < F_e(T) + \frac{2G}{9K}\frac{T - I^{Trial}_{1,n+1}}{dF_e(T)/dI_1} \tag{32}$$

3.2.4. Loading in the cap mode

Loading within the cap region requires that $f_{2,n+1}^{Trial} > 0$, $\Delta\gamma_{2,n+1} > 0$ and $\Delta\gamma_{1,n+1} = \Delta\gamma_{3,n+1} = 0$. ($16_1$), (3) and (4) give

$$\Delta \mathbf{e}_{n+1}^{P} = \Delta\gamma_{2,n+1}\frac{\partial f_{2,n+1}}{\partial \mathbf{s}_{n+1}} = \Delta\gamma_{2,n+1}\frac{\mathbf{s}_{n+1}}{F_c(|\mathbf{s}_{n+1}|, I_{1,n+1}, \kappa_{n+1})}$$

$$\Delta I_{1,n+1}^{P} = 3\Delta\gamma_{2,n+1}\frac{\partial f_{2,n+1}}{\partial I_{1,n+1}} = \Delta\gamma_{2,n+1}\frac{3(I_{1,n+1} - \kappa_{n+1})}{R^2 F_c(|\mathbf{s}_{n+1}|, I_{1,n+1}, \kappa_{n+1})} \tag{33}$$

Substituting (33) into (21), using (3), (4) and (23), yields

$$\begin{aligned} |\mathbf{s}_{n+1}| &= |\mathbf{s}_{n+1}^{Trial}| - 2G\Delta\gamma_{2,n+1}\frac{|\mathbf{s}_{n+1}|}{F_c(|\mathbf{s}_{n+1}|, I_{1,n+1}, \kappa_{n+1})} \\ I_{1,n+1} &= I_{1,n+1}^{Trial} - 9K\Delta\gamma_{2,n+1}\frac{I_{1,n+1} - \kappa_{n+1}}{R^2 F_c(|\mathbf{s}_{n+1}|, I_{1,n+1}, \kappa_{n+1})} \\ F_c(|\mathbf{s}_{n+1}|, I_{1,n+1}, \kappa_{n+1}) &- F_e(\kappa_{n+1}) = 0 \end{aligned} \tag{34}$$

Eqs.(34) provide three equations in the unknowns $|\mathbf{s}_{n+1}|$, $I_{1,n+1}$, $\Delta\gamma_{2,n+1}$ and κ_{n+1}. The hardening law ((11) and (12)) and application of an implicit backward Euler scheme give the fourth equation

$$\Delta I_{1,n+1}^{P} = W(exp^{-DX(\kappa_n)} - \exp^{-DX(\kappa_{n+1})}) = H(\kappa_{n+1}) \tag{35}$$

(34) and (35) can be reduced to one nonlinear scalar equation for κ_{n+1} which can be solved by a Newton iteration technique. Accordingly, using (34_3) in (34_2) and (34_1) yields

$$\begin{aligned} |\mathbf{s}_{n+1}| &= \frac{|\mathbf{s}_{n+1}^{Trial}|}{1 + \dfrac{2G\Delta\gamma_{2,n+1}}{F_e(\kappa_{n+1})}} \\ I_{1,n+1} - \kappa_{n+1} &= \frac{I_{1,n+1}^{Trial} - \kappa_{n+1}}{1 + \dfrac{9K\Delta\gamma_{2,n+1}}{R^2 F_e(\kappa_{n+1})}} \end{aligned} \tag{36}$$

Inserting (36) into (34_3) one obtains

$$\left\{\left[\frac{|\mathbf{s}_{n+1}^{Trial}|\, F_e(\kappa_{n+1})}{F_e(\kappa_{n+1}) + 2G\Delta\gamma_{2,n+1}}\right]^2 + \left[\frac{I_{1,n+1}^{Trial} - \kappa_{n+1}}{R + 9K\Delta\gamma_{2,n+1}/(R\, F_e(\kappa_{n+1}))}\right]^2\right\}^{1/2} - F_e(\kappa_{n+1}) = 0 \tag{37}$$

A relationship between $\Delta\gamma_{2,n+1}$ and κ_{n+1} is obtained by combining (33_2), (34_3) and (35) to give

$$\Delta\gamma_{2,n+1} = \frac{R^2 H(\kappa_{n+1}) F_e(\kappa_{n+1})}{3(I_{1,n+1} - \kappa_{n+1})} \tag{38}$$

Finally, inserting (35) into (21_2) yields

$$I_{1,n+1} = I_{1,n+1}^{Trial} - 3KH(\kappa_{n+1}) \tag{39}$$

Substitution of (39) into (38) and inserting the result into (37) gives the desired scalar nonlinear equation in terms of κ_{n+1}. In (38) it can easily be seen that the denominator is zero if $I_{1,n+1} = \kappa_{n+1}$. Since in this case (34_2) leads to $I_{1,n+1} = I_{1,n+1}^{Trial}$ and subsequently (39) gives $\kappa_{n+1} = \kappa_n$, the right hand side of (38) is an indeterminate expression. However, since κ_{n+1} now is known a priori, $\Delta\gamma_{2,n+1}$ can be obtained from (37) as

$$\Delta\gamma_{2,n+1} = \frac{|\mathbf{s}_{n+1}^{Trial}| - F_e(\kappa_n)}{2G} \quad \text{if } I_{1,n+1}^{Trial} = \kappa_n \tag{40}$$

3.2.5. Loading in the compressive corner region

Loading within this region requires that $\Delta\gamma_{1,n+1} > 0$, $\Delta\gamma_{2,n+1} > 0$ and $\Delta\gamma_{3,n+1} = 0$. From the hardening law it follows that the failure envelope and the cap behave as in ideal plasticity. Therefore the final stress point must lie at the intersection of the cap and the failure envelope

$$I_{1,n+1} = \kappa_n, \quad |\mathbf{s}_{n+1}| = F_e(\kappa_n) \tag{41}$$

Application of the generalized flow rule (16_1) and consideration of (41) yields

$$\begin{aligned} \Delta\mathbf{e}_{n+1}^P &= (\Delta\gamma_{1,n+1} + \Delta\gamma_{2,n+1})\mathbf{n}_{n+1} \\ \Delta I_{1,n+1}^P &= -3\Delta\gamma_{1,n+1}\frac{dF_e(\kappa_n)}{dI_1} \end{aligned} \tag{42}$$

Inserting (41) and (42) into (21) and considering (23) give

$$\begin{aligned} \Delta\gamma_{1,n+1} &= \frac{\kappa_n - I_{1,n+1}^{Trial}}{9K\, dF_e(\kappa_n)/dI_1} \\ \Delta\gamma_{2,n+1} &= \frac{|\mathbf{s}_{n+1}^{Trial}| - F_e(\kappa_n)}{2G} - \Delta\gamma_{1,n+1} \end{aligned} \tag{43}$$

Finally, enforcing $\Delta\gamma_{1,n+1} > 0$ and $\Delta\gamma_{3,n+1} > 0$ one obtains the inequalities that characterize loading within the corner region at $I_1 = \kappa$

$$\begin{aligned} I_{1,n+1}^{Trial} &< \kappa_n \\ |\mathbf{s}_{n+1}^{Trial}| &> F_e(\kappa_n) + \frac{2G}{9K}\frac{\kappa_n - I_{1,n+1}^{Trial}}{dF_e(\kappa_n)/dI_1} \end{aligned} \tag{44}$$

3.2.6. Update of the hardening parameter

Since for the cap κ_{n+1} is calculated directly and for the compressive corner $\kappa_{n+1} = \kappa_n$ the update procedure for the hardening parameter described in this section applies only for the failure envelope, the tension cutoff and the tensile corner mode. In (35) $\Delta\bar{I}^P_{1,n+1}$ is now a fixed, known quantity and thus, if κ_{n+1} is replaced by $\bar{\kappa}_{n+1}$, (35) is a nonlinear equation in $\bar{\kappa}_{n+1}$, which can be solved by a Newton iteration technique. Once $\bar{\kappa}_{n+1}$ is known, certain limitations on the cap movement need to be considered.

i) According to Sandler and Rubin [7] shrinkage of the cap is limited to $\kappa = 0$.

ii) To prevent the cap from overtaking the stress point on the failure envelope and thus preventing softening behavior κ_{n+1} is set to $\kappa_{n+1} = max(\bar{\kappa}_{n+1}, I_{1,n+1})$

iii) According to Sandler and Rubin [7] for the "rock" material the cap is prevented from retracting, setting $\kappa_{n+1} = max(\kappa_n, \kappa_{n+1})$ and thus allowing large amounts of dilatancy, as observed in rocks.

If none of the above limitations apply, then $\kappa_{n+1} = \bar{\kappa}_{n+1}$.

3.3. Consistent Elastoplastic Tangent Moduli

Use of tangent moduli, consistent with the integration algorithm is essential in order to preserve the quadratic rate of convergence that characterizes Newton methods (see Simo and Taylor [11]). In contrast to contiuum elastoplastic tangent moduli, which are obtained by enforcing the consistency condition on the contiuum problem, consistent algorithmic tangent moduli are obtained by enforcing consistency on the discrete algorithmic problem. Let us first deal with the easier case of ideal plasticity, which applies for all the regions of the cap model except for the cap itself. We then turn to the strain hardening cap, characterized by a yield surface which is a function of σ and the hardening parameter κ.

3.3.1. Consistent tangent moduli for regions characterized by ideal plastic behavior

Differentiation of the elastic stress-strain relationship (16_3) and the discrete flow rule (16_1) yields (see Simo et al. [8])

$$d\sigma_{n+1} = \mathbf{C} : (d\epsilon_{n+1} - d\epsilon^P_{n+1})$$

$$d\epsilon^P_{n+1} = \sum_{i=1}^{3} (d\Delta\gamma_{i,n+1} \frac{\partial f_{i,n+1}}{\partial \sigma_{n+1}} + \Delta\gamma_{i,n+1} \frac{\partial^2 f_{i,n+1}}{\partial \sigma^2_{n+1}} : d\sigma_{n+1}) \tag{45}$$

Combining these two equations gives

$$d\sigma_{n+1} = \Xi_{n+1} : (d\epsilon_{n+1} - \sum_{i=1}^{3} d\Delta\gamma_{i,n+1} \frac{\partial f_{i,n+1}}{\partial \sigma_{n+1}})$$

where

$$\Xi_{n+1} = \left[\mathbf{C}^{-1} + \sum_{i=1}^{3} \Delta\gamma_{i,n+1} \frac{\partial^2 f_{i,n+1}}{\partial \sigma^2_{n+1}} \right]^{-1} \tag{46}$$

In (46_1) the coefficients $d\Delta\gamma_{i,n+1}$ are obtained by differentiating $f_{i,n+1} = 0$

$$\frac{\partial f_{j,n+1}}{\partial \sigma_{n+1}} : d\sigma_{n+1} = 0, \quad j \in J_{act} \tag{47}$$

where $j \in J_{act}$ indicates that only active yield functions, for which $\Delta\gamma_{j,n+1} > 0$ holds, are differentiated. Substituting (46_1) into (47) yields a system of m equations for the coefficients $\Delta\gamma_{i,n+1}$ of m active yield conditions. Accordingly,

$$\sum_i \frac{\partial f_{j,n+1}}{\partial \sigma_{n+1}} : \Xi_{n+1} : \frac{\partial f_{i,n+1}}{\partial \sigma_{n+1}} d\Delta\gamma_{i,n+1} = \frac{\partial f_{j,n+1}}{\partial \sigma_{n+1}} : \Xi_{n+1} : d\epsilon_{n+1} \qquad i,j \in J_{act} \tag{48}$$

Rearranging terms in (48) gives

$$\sum_i g_{ji,n+1}\, d\Delta\gamma_{i,n+1} = \frac{\partial f_{j,n+1}}{\partial \sigma_{n+1}} : \Xi_{n+1} : d\epsilon_{n+1} \,,$$

where

$$g_{ji,n+1} = \frac{\partial f_{j,n+1}}{\partial \sigma_{n+1}} : \Xi_{n+1} : \frac{\partial f_{i,n+1}}{\partial \sigma_{n+1}} \qquad i,j \in J_{act} \tag{49}$$

which leads to

$$d\Delta\gamma_{i,n+1} = \sum_j g^{-1}_{ij,n+1} \left(\frac{\partial f_{j,n+1}}{\partial \sigma_{n+1}} : \Xi_{n+1} : d\epsilon_{n+1} \right) \tag{50}$$

where $g^{-1}_{ij,n+1}$ are the coefficients of the inverse of the matrix $\mathbf{g}_{n+1}$. Finally, inserting (50) into (46_1) one obtains the expression for the consistent tangent moduli for multisurface ideal plasticity

$$\frac{d\sigma_{n+1}}{d\epsilon_{n+1}} = \Xi_{n+1} - \sum_i \sum_j g^{-1}_{ij,n+1}\, \mathbf{N}_{i,n+1} \otimes \mathbf{N}_{j,n+1}$$

where

$$\mathbf{N}_{i,n+1} = \Xi_{n+1} : \frac{\partial f_{i,n+1}}{\partial \sigma_{n+1}} \qquad i,j \in J_{act} \tag{51}$$

3.3.2. Consistent Tangent Moduli for the Cap Mode

For the cap mode $f_2 = f_2(\sigma, \kappa)$ and (45_2) is replaced by

$$d\epsilon^p_{n+1} = d\Delta\gamma_{2,n+1} \frac{\partial f_{2,n+1}}{\partial \sigma_{n+1}} + \Delta\gamma_{2,n+1} \left(\frac{\partial^2 f_{2,n+1}}{\partial \sigma^2_{n+1}} : d\sigma_{n+1} + \frac{\partial^2 f_{2,n+1}}{\partial \sigma_{n+1}\, \partial \kappa_{n+1}} d\kappa_{n+1} \right) \tag{52}$$

Inserting (52) into (45_1) yields

$$d\sigma_{n+1} = \Xi_{n+1} : d\epsilon_{n+1} - \Xi_{n+1} : \frac{\partial f_{2,n+1}}{\partial \sigma_{n+1}} d\Delta\gamma_{2,n+1} - \Delta\gamma_{2,n+1}\Xi_{n+1} : \frac{\partial^2 f_{2,n+1}}{\partial \sigma_{n+1}\partial \kappa_{n+1}} d\kappa_{n+1} \quad (53)$$

Since only one yield function is active, the sum over the active yield conditions has been omitted. Differentiation of $f_2(\sigma_{n+1},\kappa_{n+1}) = 0$ gives

$$\frac{\partial f_{2,n+1}}{\partial \sigma_{n+1}} : d\sigma_{n+1} + \frac{\partial f_{2,n+1}}{\partial \kappa_{n+1}} d\kappa_{n+1} = 0 \quad (54)$$

Rewriting (38) using (33_2) and (34_3) yields

$$\frac{1}{3} H(\kappa_{n+1}) - \Delta\gamma_{2,n+1} \frac{\partial f_{2,n+1}}{\partial I_{1,n+1}} = 0$$

and differentiation of this equation leads to the third equation for the determination of the consistent tangent moduli for the cap

$$\begin{aligned} &\frac{1}{3} \frac{dH(\kappa_{n+1})}{d\kappa_{n+1}} d\kappa_{n+1} - d\Delta\gamma_{2,n+1} \frac{\partial f_{2,n+1}}{\partial I_{1,n+1}} \\ &- \Delta\gamma_{2,n+1} \left(\frac{\partial^2 f_{2,n+1}}{\partial I_{1,n+1}\partial \sigma_{n+1}} : d\sigma_{n+1} + \frac{\partial^2 f_{2,n+1}}{\partial I_{1,n+1}\partial \kappa_{n+1}} d\kappa_{n+1} \right) = 0 \end{aligned} \quad (55)$$

Substitution of (53) into (54) and (55) leads to

$$\begin{aligned} d\Delta\gamma_{2,n+1} &= a^{-1}_{11,n+1} \frac{\partial f_{2,n+1}}{\partial \sigma_{n+1}} : \Xi_{n+1} : d\epsilon_{n+1} + a^{-1}_{12,n+1} \frac{\partial^2 f_{2,n+1}}{\partial \sigma_{n+1}\partial \kappa_{n+1}} : \Xi_{n+1} : d\epsilon_{n+1} \\ \Delta\gamma_{2,n+1} d\kappa_{n+1} &= a^{-1}_{21,n+1} \frac{\partial f_{2,n+1}}{\partial \sigma_{n+1}} : \Xi_{n+1} : d\epsilon_{n+1} + a^{-1}_{22,n+1} \frac{\partial^2 f_{2,n+1}}{\partial \sigma_{n+1}\partial \kappa_{n+1}} : \Xi_{n+1} : d\epsilon_{n+1} \end{aligned} \quad (56)$$

where the coefficients $a^{-1}_{ij,n+1}$, i,j = 1,2, are the components of the inverse of a matrix $\mathbf{a}_{n+1}$. The coefficients of $\mathbf{a}_{n+1}$ are given by

$$\begin{aligned} a_{11,n+1} &= \frac{\partial f_{2,n+1}}{\partial \sigma_{n+1}} : \Xi_{n+1} : \frac{\partial f_{2,n+1}}{\partial \sigma_{n+1}} \\ a_{12,n+1} &= \frac{\partial f_{2,n+1}}{\partial \sigma_{n+1}} : \Xi_{n+1} : \frac{\partial^2 f_{2,n+1}}{\partial \sigma_{n+1}\partial \kappa_{n+1}} - \frac{1}{\Delta\gamma_{2,n+1}} \frac{\partial f_{2,n+1}}{\partial \kappa_{n+1}} \\ a_{21,n+1} &= \frac{\partial^2 f_{2,n+1}}{\partial \sigma_{n+1}\partial \kappa_{n+1}} : \Xi_{n+1} : \frac{\partial f_{2,n+1}}{\partial \sigma_{n+1}} + \frac{1}{\Delta\gamma_{2,n+1}} \frac{\partial f_{2,n+1}}{\partial I_{1,n+1}} \end{aligned} \quad (57)$$

$$a_{22,n+1} = \frac{\partial^2 f_{2,n+1}}{\partial \sigma_{n+1} \partial \kappa_{n+1}} : \Xi_{n+1} : \frac{\partial^2 f_{2,n+1}}{\partial \sigma_{n+1} \partial \kappa_{n+1}} + \frac{1}{\Delta \gamma_{2,n+1}} \frac{\partial^2 f_{2,n+1}}{\partial I_{1,n+1} \partial \kappa_{n+1}} - \frac{1}{3\Delta \gamma_{2,n+1}^2} \frac{dH(\kappa_{n+1})}{d\kappa_{n+1}}$$

In (56) and (57) use of

$$\frac{\partial^2 f_{2,n+1}}{\partial I_{1,n+1} \partial \sigma_{n+1}} = -\frac{\partial^2 f_{2,n+1}}{\partial \kappa_{n+1} \partial \sigma_{n+1}}$$

has been made. Finally, inserting (56) into (53) gives the expression for the consistent tangent moduli for the cap mode

$$\frac{d\sigma_{n+1}}{d\epsilon_{n+1}} = \Xi_{n+1} - \sum_{i=1}^{2} \sum_{j=1}^{2} a_{ij,n+1}^{-1} \mathbf{N}_{i,n+1} \otimes \mathbf{N}_{j,n+1} \tag{58}$$

where

$$\mathbf{N}_{1,n+1} = \Xi_{n+1} : \frac{\partial f_{2,n+1}}{\partial \sigma_{n+1}}, \qquad \mathbf{N}_{2,n+1} = \Xi_{n+1} : \frac{\partial^2 f_{2,n+1}}{\partial \sigma_{n+1} \partial \kappa_{n+1}}$$

and

$$\frac{\partial^2 f_{2,n+1}}{\partial \sigma_{n+1} \partial \kappa_{n+1}} = \frac{(I_{1,n+1} - \kappa_{n+1}) \mathbf{s}_{n+1} - |\mathbf{s}_{n+1}|^2 \mathbf{1}}{R^2 F_e^3(\kappa_{n+1})} .$$

Note, that because of $a_{12,n+1} \neq a_{21,n+1}$ or more precisely because of

$$\frac{\partial f_{2,n+1}}{\partial \kappa_{n+1}} \neq -\frac{\partial f_{2,n+1}}{\partial I_{1,n+1}}$$

where

$$\frac{\partial f_{2,n+1}}{\partial I_{1,n+1}} = \frac{I_{1,n+1} - \kappa_{n+1}}{R^2 F_c(|\mathbf{s}_{n+1}|, I_{1,n+1}, \kappa_{n+1})}$$

and

$$\frac{\partial f_{2,n+1}}{\partial \kappa_{n+1}} = -\frac{\partial f_{2,n+1}}{\partial I_{1,n+1}} - \frac{dF_e(\kappa_{n+1})}{d\kappa_{n+1}} \tag{59}$$

the tensor of the consistent tangent moduli is not symmetric. The asymmetry is caused by the fact, that the cap model does not obey the principle of maximum plastic dissipation, which, as shown by Simo and Hughes [10], implies not only associativity of the flow rule but also of the hardening law. For the cap model these conditions imply

$$\dot{\epsilon}^P = \sum_{i=1}^{3} \dot{\gamma}_i \frac{\partial f_i}{\partial \sigma}, \qquad \dot{\kappa} = -\sum_{i=1}^{3} \dot{\gamma}_i D_i(\kappa) \frac{\partial f_i}{\partial \kappa} , \tag{60}$$

where $D_i(\kappa)$ is the plastic modulus. From (11) and (12) a rate form of the hardening law for the cap model is given by

$$\dot{\kappa} = 3\dot{\gamma} \frac{1}{WD \dfrac{dX(\kappa)}{d\kappa} \exp^{-DX(\kappa)}} \frac{\partial f_2}{\partial I_1} \tag{61}$$

Noting that only f_2 depends on κ from (60_2) it follows that

$$\dot{\kappa} = -\dot{\gamma}_2 D_2(\kappa) \frac{\partial f_2(\sigma,\kappa)}{\partial \kappa} \quad , \tag{62}$$

and therefore the commonly accepted hardening law for the cap model is nonassociative and leads to unsymmetric tangent operators. To overcome the drawback of unsymmetric tangent moduli an associative hardening law, only permitting expansion of the cap, will be presented in section 4.

3.3.3. Algebraic inversion of Ξ_{n+1}^{-1}

In a finite element implementation of the cap model the numerical inversion of the expression

$$\left[\mathbf{C}^{-1} + \sum_{i=1}^{3} \Delta\gamma_{i,n+1} \frac{\partial^2 f_{i,n+1}}{\partial \sigma_{n+1}^2} \right]^{-1}$$

to obtain the algorithmic moduli Ξ_{n+1} (46_2) needs to be done for each integration point in each iteration step. This inversion can be done algebraically applying the Sherman-Morrison formula. To this end let us first deal with the smooth regions of the yield surface, where only one yield condition is active. The second derivatives of the yield functions with respect to σ are

$$\begin{aligned}
\frac{\partial^2 f_{1,n+1}}{\partial \sigma_{n+1}^2} &= \frac{1}{|\mathbf{s}_{n+1}|} \left(\mathbf{I}_{Dev} - \mathbf{n}_{n+1} \otimes \mathbf{n}_{n+1} \right) - \frac{d^2 F_e}{dI_{1,n+1}^2} \mathbf{1} \otimes \mathbf{1} \\
\frac{\partial^2 f_{2,n+1}}{\partial \sigma_{n+1}^2} &= \frac{1}{F_e(\kappa_{n+1})} \left(\mathbf{I}_{Dev} - \frac{\partial f_{2,n+1}}{\partial \sigma_{n+1}} \otimes \frac{\partial f_{2,n+1}}{\partial \sigma_{n+1}} + \frac{1}{R^2} \mathbf{1} \otimes \mathbf{1} \right) \\
\frac{\partial^2 f_{3,n+1}}{\partial \sigma_{n+1}^2} &= \mathbf{0}
\end{aligned} \tag{63}$$

where $\mathbf{I}_{Dev}$ is defined by $\mathbf{s} = \mathbf{I}_{Dev} : \sigma$. Therefore for both the failure envelope mode and the cap mode the basic structure of Ξ_{n+1} is

$$\Xi_{n+1} = \left[\mathbf{C}^{-1} + c_1 \mathbf{I}_{Dev} + c_2 \mathbf{1} \otimes \mathbf{1} - c_1 \mathbf{p} \otimes \mathbf{p} \right]^{-1} \tag{64}$$

For the failure envelope c_1, c_2, and $\mathbf{p}$ in (64) are given by

$$c_1 = \frac{\Delta\gamma_{1,n+1}}{|\mathbf{s}_{n+1}|}, \qquad c_2 = -\Delta\gamma_{1,n+1} \frac{d^2 F_e}{dI_{1,n+1}^2}, \qquad \mathbf{p} = \mathbf{n}_{n+1}$$

whereas for the cap

$$c_1 = \frac{\Delta\gamma_{2,n+1}}{F_e(\kappa_{n+1})}, \quad c_2 = \frac{c_1}{R^2}, \quad \mathbf{p} = \frac{\partial f_{2,n+1}}{\partial\sigma_{n+1}}$$

For the tension cutoff mode use of (63_3) gives Ξ_{n+1} is equal to C.

Inserting

$$\mathbf{A}^{-1} = \mathbf{C}^{-1} + c_1\mathbf{I}_{Dev} + c_2\,\mathbf{1}\otimes\mathbf{1} \tag{65}$$

into (64) and applying the Sherman-Morrison formula one obtains

$$\Xi_{n+1} = \mathbf{A} - \frac{\mathbf{A}:\mathbf{p}\otimes\mathbf{A}:\mathbf{p}}{\mathbf{p}:\mathbf{A}:\mathbf{p} - \dfrac{1}{c_1}}. \tag{66}$$

Note that the inversion of $\mathbf{A}^{-1}$ to obtain A can also easily be done algebraically. Even for the corner regions the basic structure of Ξ_{n+1} remains unchanged. Because of (63_3), Ξ_{n+1} for the tensile corner mode is identical with Ξ_{n+1} for the failure envelope mode. For the compressive corner, because of (41), one obtains

$$F_e(\kappa_{n+1}) = F_e(\kappa_n) = |\mathbf{s}_{n+1}|, \quad \frac{\partial f_{2,n+1}}{\partial\sigma_{n+1}} = \mathbf{n}_{n+1}. \tag{67}$$

Inserting (67) into (63_2) and combining (63_1) and (63_2) yields (64) where now

$$c_1 = \frac{\Delta\gamma_{1,n+1} + \Delta\gamma_{2,n+1}}{F_e(\kappa_n)}, \quad c_2 = -\Delta\gamma_{1,n+1}\frac{d^2F_e}{dI_{1,n+1}^2} + \frac{\Delta\gamma_{2,n+1}}{R^2F_e(\kappa_n)}, \quad \mathbf{p} = \mathbf{n}_{n+1} \tag{68}$$

4. AN ASSOCIATIVE HARDENING LAW FOR THE CAP MODEL

In order to formulate an associative hardening law (60_2) is obtained by analogy with Koiter's generalized flow rule for nonsmooth multisurface plasticity. The f_1 and f_3 given by (1) and (5), respectively, do not depend on the hardening parameter κ. Hence, from (62), it is not possible to formulate an associative hardening law, permitting contraction of the cap, without changing the yield functions f_1 and f_3. In other words, for an associative hardening law contraction of the cap can only be modelled, if f_1 and f_3 also depend on the hardening parameter κ. Therefore this chapter only deals with the case of an expanding cap, which, as pointed out by Sandler and Rubin [7] applies to the material rock. In (62) the plastic modulus $D_2(\kappa)$ is chosen as

$$D_2(\kappa) = \frac{1}{W_a D_a \dfrac{dX(\kappa)}{d\kappa}\exp^{-D_a X(\kappa)}}$$

and D_a and W_a are the hardening parameters for the associative hardening law. Integration of (62) by a backward Euler method and rearranging terms yields

$$\frac{\Delta\kappa_{n+1}}{D_2(\kappa_{n+1})} + \Delta\gamma_{2,n+1}\frac{\partial f_{2,n+1}}{\partial\kappa_{n+1}} = 0 \tag{69}$$

(69) and (37) can be solved by means of a Newton iteration technique to obtain $\Delta\gamma_{2,n+1}$ and κ_{n+1}. For the determination of the consistent tangent moduli linearization of (69) gives

$$\frac{D_2(\kappa_{n+1}) + \Delta\kappa_{n+1}\dfrac{dD_2(\kappa_{n+1})}{d\kappa_{n+1}}}{D_2^2(\kappa_{n+1})} d\kappa_{n+1} + \frac{\partial f_{2,n+1}}{\partial\kappa_{n+1}} d\Delta\gamma_{2,n+1}$$

$$+ \Delta\gamma_{2,n+1}\left(\frac{\partial^2 f_{2,n+1}}{\partial\kappa_{n+1}\partial\sigma_{n+1}} : d\sigma_{n+1} + \frac{\partial^2 f_{2,n+1}}{\partial\kappa_{n+1}^2} d\kappa_{n+1}\right) = 0 \tag{70}$$

Eq.(70) replaces (55). Combining (53), (54) and (70) again yields (56), but now in contrast to (57_3) and (57_4) one obtains

$$a_{21,n+1} = a_{12,n+1} = \frac{\partial f_{2,n+1}}{\partial\sigma_{n+1}} : \Xi_{n+1} : \frac{\partial^2 f_{2,n+1}}{\partial\sigma_{n+1}\partial\kappa_{n+1}} - \frac{1}{\Delta\gamma_{2,n+1}}\frac{\partial f_{2,n+1}}{\partial\kappa_{n+1}}$$

$$a_{22,n+1} = \frac{\partial^2 f_{2,n+1}}{\partial\sigma_{n+1}\partial\kappa_{n+1}} : \Xi_{n+1} : \frac{\partial^2 f_{2,n+1}}{\partial\sigma_{n+1}\partial\kappa_{n+1}} - \frac{1}{\Delta\gamma_{2,n+1}}\frac{\partial^2 f_{2,n+1}}{\partial\kappa_{n+1}^2} \tag{71}$$

$$- \frac{1}{\Delta\gamma_{2,n+1}^2}\frac{D_2(\kappa_{n+1}) + \Delta\kappa_{n+1}\dfrac{dD_2(\kappa_{n+1})}{d\kappa_{n+1}}}{D_2^2(\kappa_{n+1})}$$

where

$$\frac{\partial^2 f_{2,n+1}}{\partial\kappa_{n+1}^2} = \frac{|s_{n+1}|^2}{R^2 F_e(\kappa_{n+1})} - \frac{d^2 F_e(\kappa_{n+1})}{d\kappa_{n+1}^2}$$

It can be seen that the consistent tangent moduli are symmetric. For the associative hardening law the compressive corner point does not act as in ideal plasticity, but also exhibits hardening, when the stress point lies within this corner region. At the compressive corner

$$\frac{\partial f_1}{\partial\kappa} = 0 \quad \text{and} \quad I_{1,n+1} = \kappa_{n+1}$$

hence, the discrete hardening law for the compressive corner region follows from (59) and (69) as

$$\frac{\Delta\kappa_{n+1}}{D_2(\kappa_{n+1})} - \Delta\gamma_{2,n+1}\frac{dF_e(\kappa_{n+1})}{d\kappa_{n+1}} = 0\,. \tag{72}$$

This nonlinear scalar equation also can be solved by means of a Newton iteration technique. Once κ_{n+1} is known the consistency parameters $\Delta\gamma_{1,n+1}$ and $\Delta\gamma_{2,n+1}$ can be calculated by means of (43), if κ_n is replaced by κ_{n+1}. The consistent tangent moduli for the compressive corner region now are given by

$$\frac{d\sigma_{n+1}}{d\epsilon_{n+1}} = \Xi_{n+1} - \sum_{i=1}^{3}\sum_{j=1}^{3} a_{ij,n+1}^{-1}\, N_{i,n+1} \otimes N_{j,n+1} \tag{73}$$

where Ξ_{n+1} can be determined according to (64) and (68) (again, κ_n must to be replaced by κ_{n+1}) and

$$\mathbf{N}_{1,n+1} = \Xi_{n+1} : \frac{\partial f_{1,n+1}}{\partial \sigma_{n+1}}$$

$$\mathbf{N}_{2,n+1} = \Xi_{n+1} : \frac{\partial f_{2,n+1}}{\partial \sigma_{n+1}}$$

$$\mathbf{N}_{3,n+1} = \Xi_{n+1} : \frac{\partial^2 f_{2,n+1}}{\partial \sigma_{n+1} \partial \kappa_{n+1}}$$

and the $a^{-1}_{ij,n+1}$ are the coefficients of the inverse of a matrix $\mathbf{a}_{n+1}$. The coefficients of $\mathbf{a}_{n+1}$ are given by

$$a_{11,n+1} = \frac{\partial f_{1,n+1}}{\partial \sigma_{n+1}} : \Xi_{n+1} : \frac{\partial f_{1,n+1}}{\partial \sigma_{n+1}}$$

$$a_{12,n+1} = a_{21,n+1} = \frac{\partial f_{1,n+1}}{\partial \sigma_{n+1}} : \Xi_{n+1} : \frac{\partial f_{2,n+1}}{\partial \sigma_{n+1}}$$

$$a_{13,n+1} = a_{31,n+1} = \frac{\partial f_{1,n+1}}{\partial \sigma_{n+1}} : \Xi_{n+1} : \frac{\partial^2 f_{2,n+1}}{\partial \sigma_{n+1} \partial \kappa_{n+1}}$$

$$a_{22,n+1} = \frac{\partial f_{2,n+1}}{\partial \sigma_{n+1}} : \Xi_{n+1} : \frac{\partial f_{2,n+1}}{\partial \sigma_{n+1}}$$

$$a_{23,n+1} = a_{32,n+1} = \frac{\partial f_{2,n+1}}{\partial \sigma_{n+1}} : \Xi_{n+1} : \frac{\partial^2 f_{2,n+1}}{\partial \sigma_{n+1} \partial \kappa_{n+1}} - \frac{1}{\Delta\gamma_{2,n+1}} \frac{\partial f_{2,n+1}}{\partial \kappa_{n+1}}$$

$$a_{33,n+1} = \frac{\partial^2 f_{2,n+1}}{\partial \sigma_{n+1} \partial \kappa_{n+1}} : \Xi_{n+1} : \frac{\partial^2 f_{2,n+1}}{\partial \sigma_{n+1} \partial \kappa_{n+1}} - \frac{1}{\Delta\gamma_{2,n+1}} \frac{\partial^2 f_{2,n+1}}{\partial \kappa^2_{n+1}}$$

$$- \frac{1}{\Delta\gamma^2_{2,n+1}} \frac{D_2(\kappa_{n+1}) + \Delta\kappa_{n+1} \dfrac{dD_2(\kappa_{n+1})}{d\kappa_{n+1}}}{D^2_2(\kappa_{n+1})}$$

5. NUMERICAL EXAMPLES

5.1. Tests for the Nonassociative Hardening Law

5.1.1. Tests based on the Colorado Concrete Data

Based on the Colorado Concrete Data [13] an extensive study of the predictive capabilites of the cap model has been performed by Simo et al. [6]. The bulk modulus K and the shear modulus G are specified in [13] as 2100 ksi and 1700 ksi, respectively. The other parameters for the modified cap have been computed using the fit criteria described by Simo et al. [6]. The same tests described by Simo et al. [6] were employed for this parameter fit procedure. Table 1 contains a comparison of the parameters for the present study and those obtained by Simo et al. [6].

parameter	Simo et al. [6]	present study	unit
α	3.86	4.34	*ksi*
θ	0.11	0.33	---
λ	1.16	1.80	*ksi*
β	0.44	0.54	ksi^{-1}
R	4.43	2.89	---
D	0.0032	0.0032	ksi^{-1}
W	0.42	0.42	---
T	-0.30	-0.30	*ksi*
$X(\kappa_0)$	16.0	16.0	*ksi*

Table 1 - Parameters for Colorado Concrete

Figure 2 contains a plot of the initial yield surfaces resulting from the two different sets of parameters. The root-mean-square errors, found from backprediction, are nearly identical to the values specified by Simo et al.[6]. Based on the new parameters for the cap model the tests 1-2, 2-2 and 3-5 have been calculated and the results are nearly identical to those obtained by Simo et al. [6].

5.1.2. Plane strain, flexible footing problem

In order to demonstrate the effectiveness of the algorithm developed here, a plane strain, flexible footing problem is analyzed. The two finite element meshes, consisting of 72 four-node bilinear isoparametric quadrilateral elements and 72 nine-node quadratic Lagrangian elements, respectively, used for the calculation are shown in Figure 3. The parameters for the cap model are determined by means of an optimization procedure for the uniaxial strain test for McCormick Ranch Sand (Fig.4), given in Sandler and Rubin [7], and are listed in Table 2. $X(\kappa_0)$ was chosen as 0.175 ksi. In [7] the bulk modulus K and the shear modulus G are specified as 66.67 ksi and 40.0 ksi, respectively.

parameter	value	unit
α	0.27	*ksi*
θ	0.02	---
λ	0.17	*ksi*
β	0.67	ksi^{-1}
R	2.50	---
D	0.67	ksi^{-1}
W	0.0064	---
T	-0.30	*ksi*
$X(\kappa_0)$	0.175	*ksi*

Table 2 - Parameters for McCormick Ranch Sand

The uniformly distributed reference load is chosen as $p_0 = 0.05$ ksi. Figure 5 contains a plot of the load-displacement curves obtained by means of the two finite element meshes for the point located in the symmetry plane directly beneath the applied load. The calculation has been performed by means of the arc-length method and the termination criterion for the Newton solution strategy was chosen in terms of the energy norm E, which is computed from the residual force and the incremental displacement vector as

$$\Delta E_{n+1}^{(i)} \leq 10^{-9} \Delta E_{n+1}^{(1)}$$

where the subscript n+1 denotes the load step and the superscripts refer to the first or i-th iteration step, respectively. The number of iterations, necessary to achieve this condition never exceeded four for the four-node element and never exceeded five for the nine-node element.

5.2. Tests for the Associative Hardening Law

5.2.1. Colorado Concrete Data

Since only the hardening law has been changed, an optimization for the cap parameters only leads to new values for the parameters D and W, now called D_a and W_a, respectively. The numerical values are $D_a = 0.0086\ ksi^{-1}$ and $W_a = 0.14$. Again, with the new parameters, the tests 1-2, 2-2 and 3-5 have been calculated and there are no significant differences for the predicted stresses, compared with those obtained by Simo et al.[6]. Nevertheless it should be mentioned that, although the two different hardening laws lead to the same qualitative behavior under pure hydrostatic loading, the associative hardening law leads to a considerably different response for hydrostatic strains which are larger than those observed in the experiments. The hydrostatic range of the strains for the experiments did not exceed $tr(\epsilon) = 0.025$ and within a region which is even six times larger there is good agreement for the two different hardening laws (Fig.6). Since the hydrostatic behavior for the region $tr(\epsilon) > 0.025$ is only obtained by extrapolation and because the stresses and strains for the region $tr(\epsilon) > 0.15$ are too large for concrete there are no experimental data available for this part and the considerable differences for $tr(\epsilon) > 0.15$ (Fig.6) are only hypothetical and have no influence on the stress predictions.

5.2.2. Plane strain, flexible footing problem

The optimization procedure, based on the uniaxial strain test for McCormick Ranch Sand only changes the parameter W, now called W_a. The numerical value is $W_a = 0.031$. Both the nonassociative and the associative hardening law lead to the same shape of the hydrostatic curve, but there is a difference in the maximum amount of predicted hydrostatic plastic strains for these two hardening laws (Fig.7). However, this observation does not contradict the assumptions made by DiMaggio and Sandler [1], who pointed out that they only used the qualitative shape of the plot of the hydrostatic test results to set up the hardening law for the cap model. The differences observed for the two different hardening laws have litte influence on the load-displacement curve for the plain strain, flexible footing problem, obtained by means of the 4-node element (Fig.8).

6. CONCLUSION

An algorithmic treatment of the cap model based upon a closest point projection method has been considered in detail. Consistent algorithmic loading/unloading conditions for all possible modes of response have been formulated by exploiting the discrete Kuhn-Tucker conditions for nonsmooth multisurface plasticity.

New closest point projection algorithms have been derived for the cap and the failure envelope, characterized by reducing local iterations to the solution of a nonlinear scalar equation by a Newton method and thus exhibiting a quadratic rate of convergence, whereas the secant iteration scheme, proposed by Sandler and Rubin [7], is only superlinear.

It has been shown that the original cap model does not obey the principle of maximum plastic dissipation, because the hardening law is non-associative. This leads to the undesirable feature of unsymmetric tangent moduli. To overcome this drawback an associative hardening law, which does not permit cap contraction, has been proposed. In addition it has been pointed out, that an associative hardening law, which permits contraction of the cap, cannot be developed without changing the yield conditions for those regions which act as in ideal plasticity. Inclusion of this aspect is left to a subsequent study.

REFERENCES

[1] DiMaggio, F.L., and I.S. Sandler, " Material models for granular soils", *J. of Engng. Mech.* A.S.C.E., pp.935-950, 1971.

[2] Sandler, I.S., F.L. DiMaggio and G.Y. Baladi, "Generalized cap model for geological materials", *J. of the Geotech. Engng. Div.*, A.S.C.E., 102, No.GT7, pp.683-699, 1976.

[3] Chen, W.F., *Plasticity in Reinforced Concrete,* McGraw-Hill, New York, 1982.

[4] Chen, W.F., and G.Y. Baladi, *Soil Plasticity - Theory and Implementation* Elsevier,Amsterdam, 1985.

[5] Desai, C.S., and H.J. Siriwardane, " Constitutive laws for Engineering materials", Prentice Hall, 1984.

[6] Simo, J.C., J.W. Ju, K.S. Pister and R.L. Taylor, "An assessment of the cap model: Consistent return algorithms and rate-dependent extensions", *J. Eng. Mech., A.S.C.E., 114, No.2, pp.191-218, 1988.*

[7] Sandler, I.S., and D. Rubin, "An Algorithm and a modular subroutine for the cap model", *Int. J. Numer. Analy. Meth. Geomech.*, 3, pp. 173-186, 1979.

[8] Simo, J.C., J.G. Kennedy and S. Godvindjee, "Unconditionally stable return mapping algorithms for non-smooth multi-surface plasticity amenable to exact linearization", *Int. J. Num. Meth. Engng.*, 26, pp. 2161 - 2185, 1988.

[9] Koiter, W.T., "Stress Strain Relations, Uniqueness and Variational Theorems for Elastic-Plastic Materials with a Singular Yield Surface", *Quart. J. Appl. Math.*, 11, pp. 350-354, 1953.

[10] Simo, J.C., and T.J.R. Hughes, *Elastoplasticity and Viscoplasticity. Computational Aspects,* in press.

[11] Simo, J.C., and R.L. Taylor, "Consistent tangent operators for rate independent elastoplasticity", *Comp. Meth. Appl. Mech. Engng.*, 48, pp.101-118, 1985.

[12] Simo, J.C., and R.L. Taylor, "A return mapping algorithm for plane strain elastoplasticity", *Int. J. Num. Meth. Engng.*, 22,No.3, pp.649-670, 1986.

[13] Scavuzzo, R., T. Stankowski, K.H. Gerstle and H.Y. Ko, "Stress-Strain Curves for Concrete Under Multiaxial Load Histories", NSF CME-80-01508, Department of Civil Engineering, University of Colorado, Boulder, August 1983.

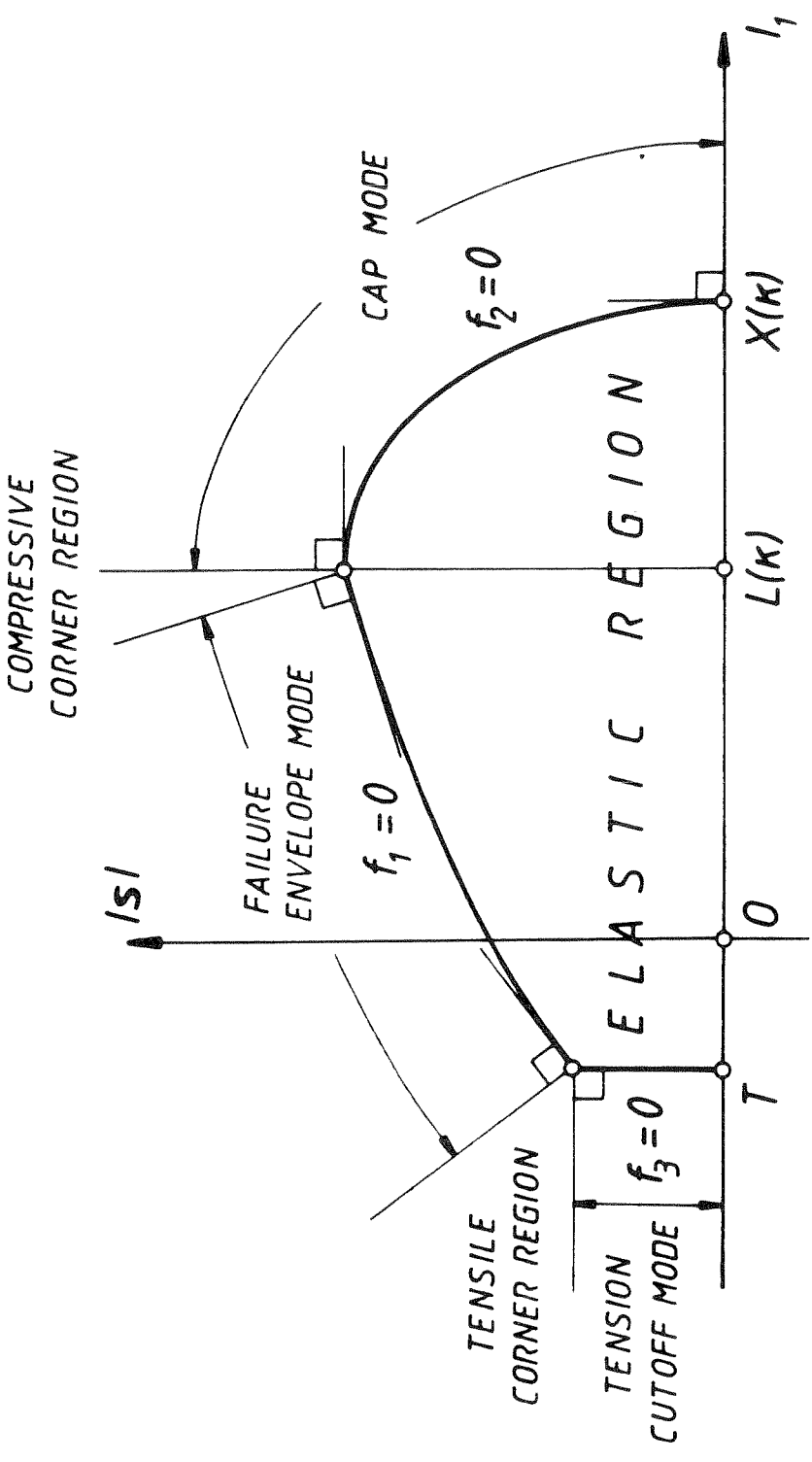

Fig.1 - The yield surface of the cap model

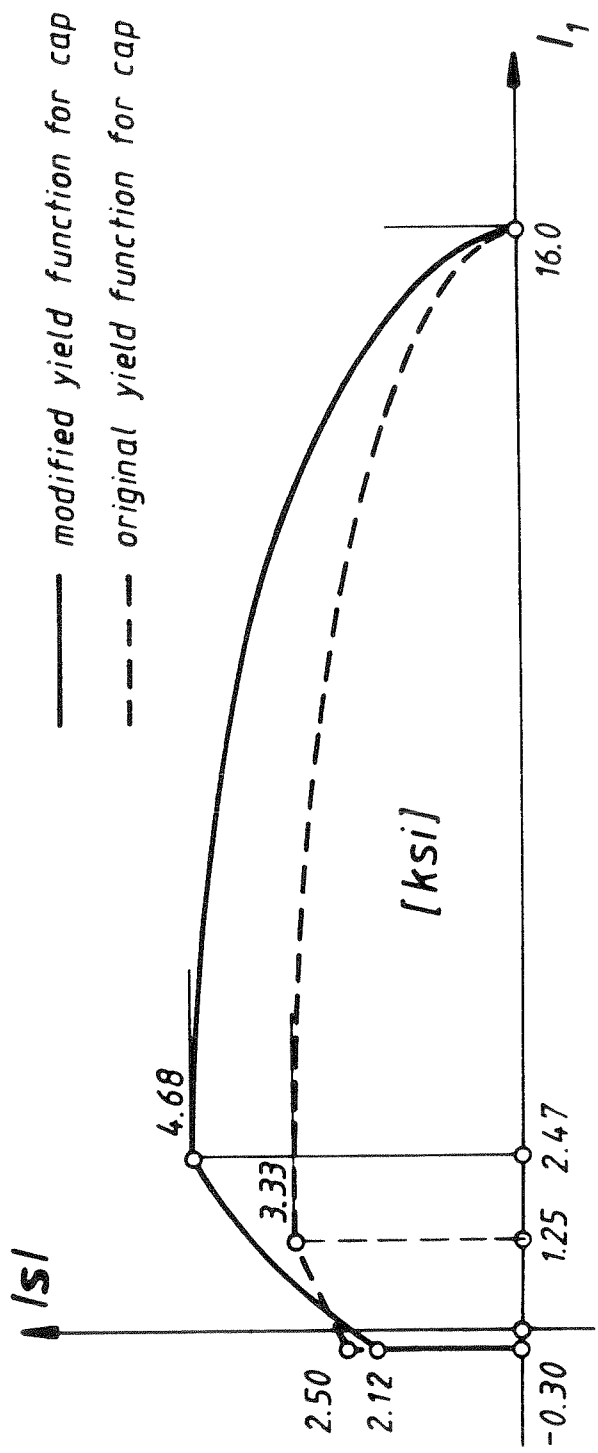

Fig.2 - Initial yield surfaces of the cap model for the different formulations of the yield conditions for the cap

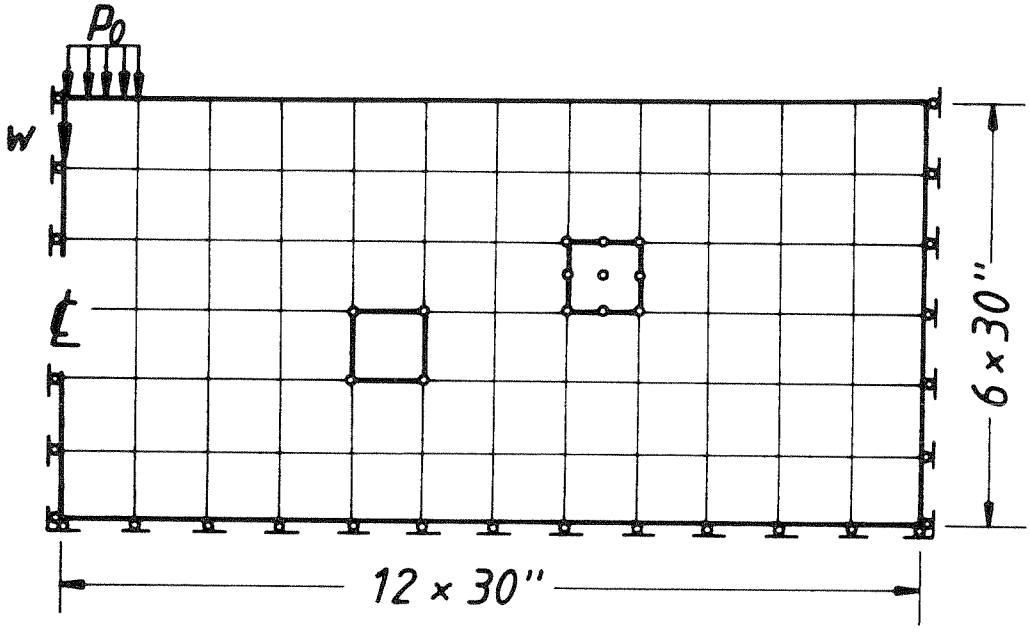

Fig.3 - plane strain, flexible footing problem

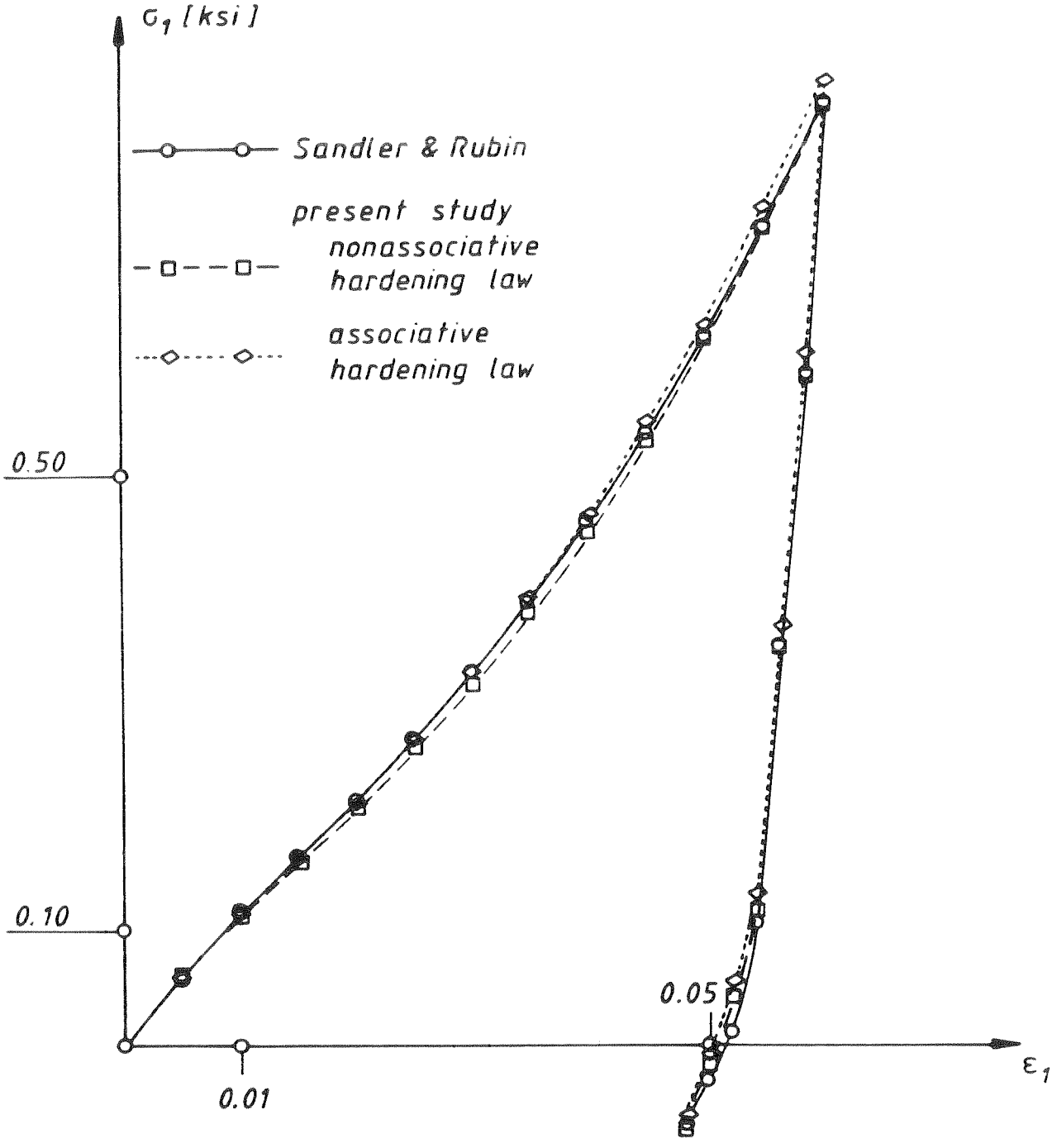

Fig.4 - Uniaxial strain test for McCormick Ranch Sand

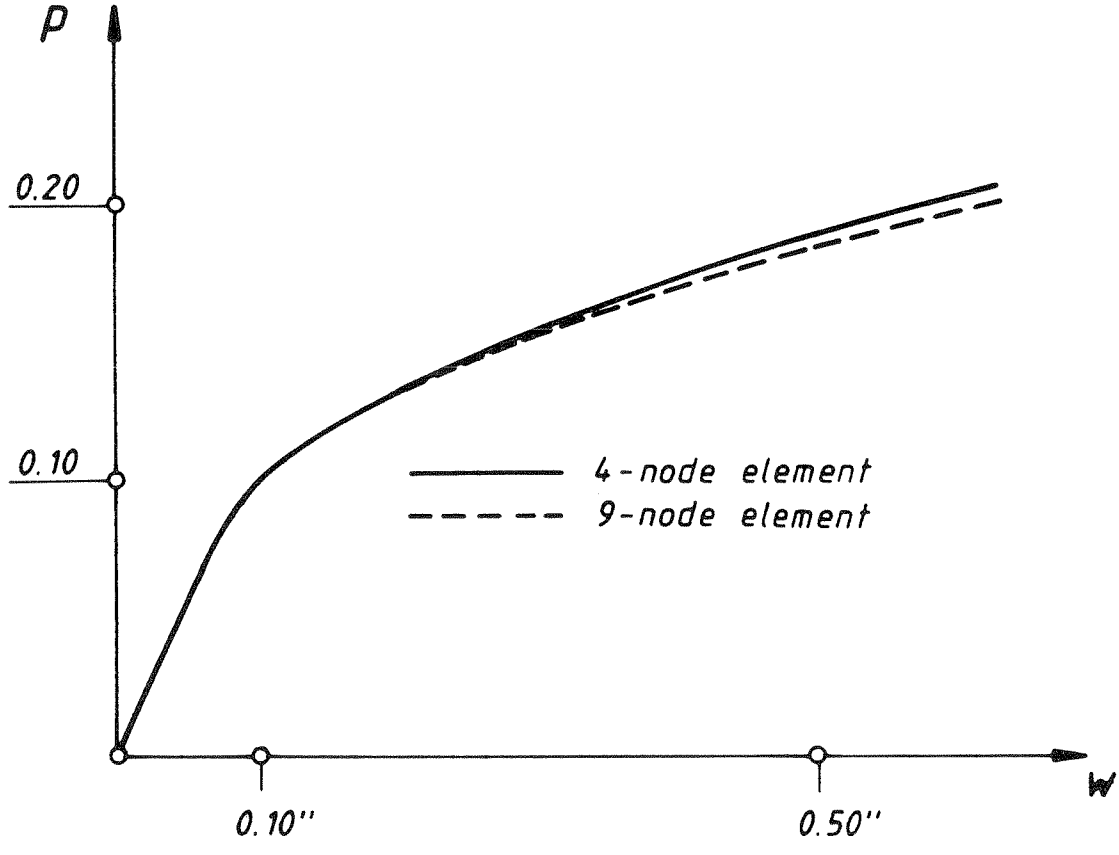

Fig.5 - Load-displacement curves for the plane strain, flexible footing problem

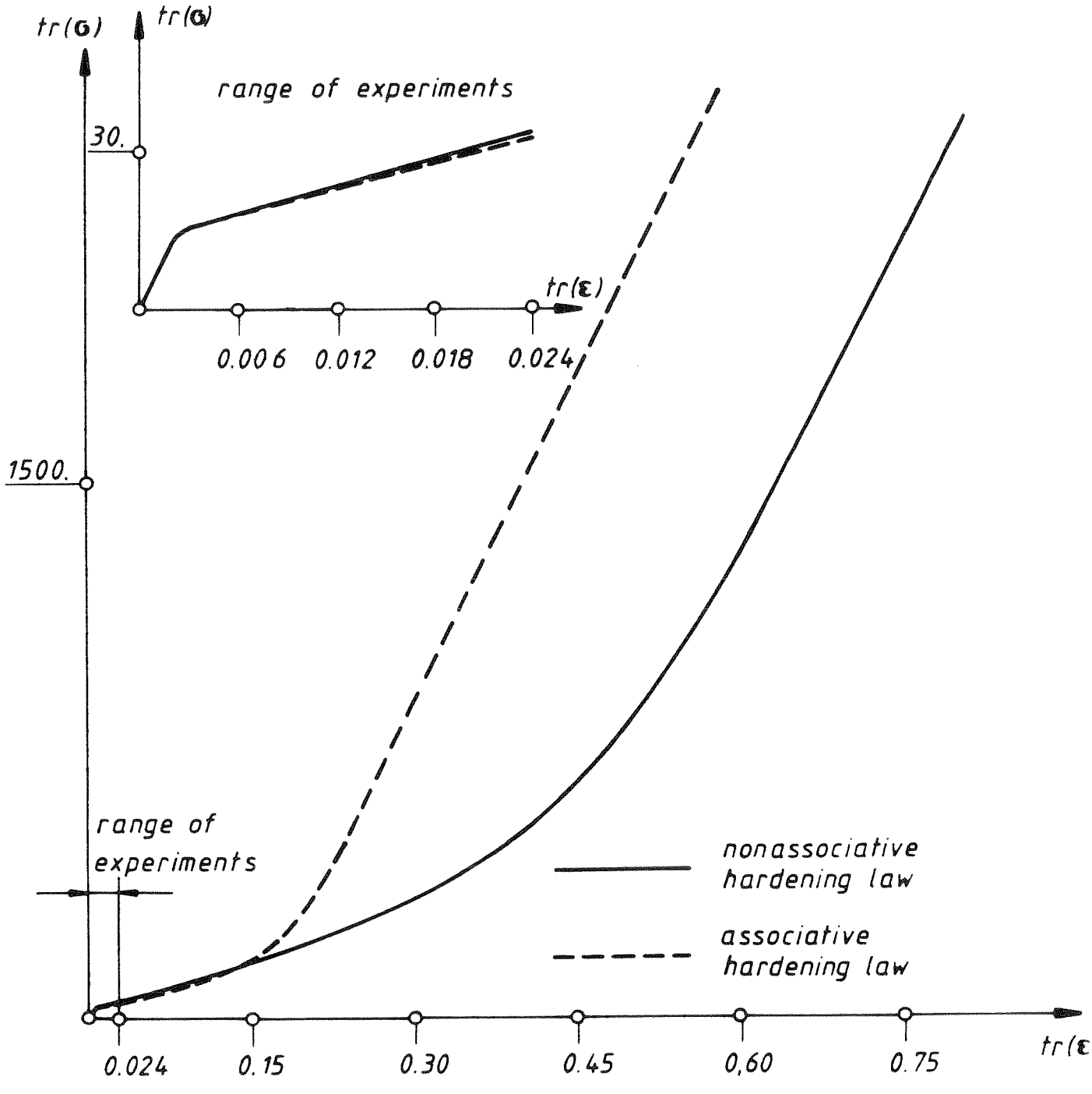

Fig.6 - Predicted hydrostatic behavior for the Colorado Conrete Data

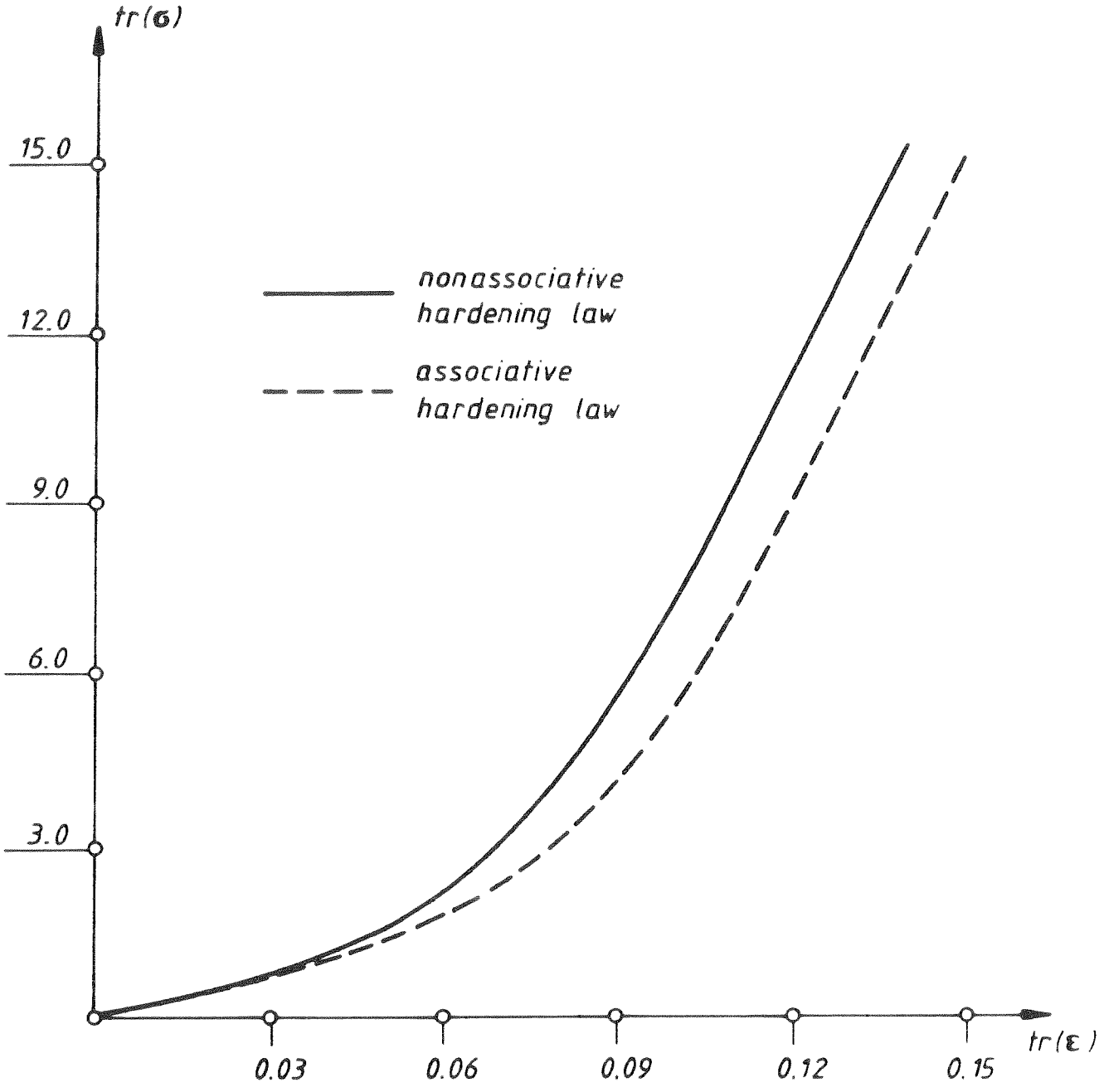

Fig.7 - Predicted hydrostatic behavior for McCormick Ranch Sand

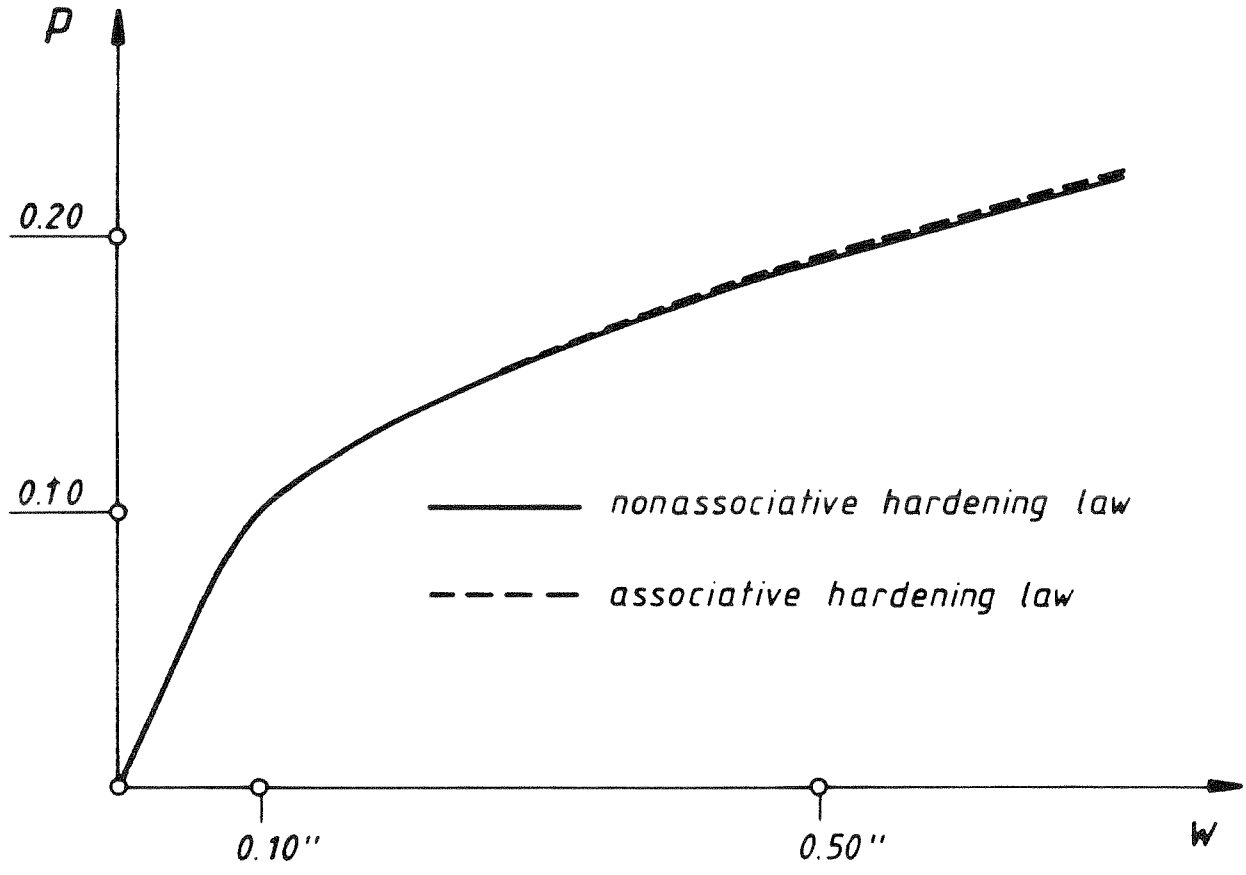

Fig.8 - Load-displacement curves for the two hardening laws (4-node element)